Multilateration Using A Priori Position Estimates

Eric Widdison, *Member, IEEE*, and David G. Long, *Life Fellow, IEEE*

***Abstract*— Existing multilateration algorithms typically do not account for information that is previously known about the target's position. This paper presents a method of using an *a priori* estimate of the target's location and planar approximations of the spheres to determine the target's position. This algorithm meets or exceeds the performance of traditional multilateration algorithms when the *a priori* position is accurate enough. It significantly out-performs traditional multilateration in wide-area multilateration scenarios, particularly in the typical case where the reference points are nearly coplanar.**

***Index Terms*— TDOA, multilateration, localization, algorithm.**

I. Introduction

MULTILATERATION is a process whereby an unknown position of an object can be determined using the distance between its location and several known points. The unknown location lies at the intersection of the spheres centered at the known points with the corresponding radii.

One application of this is to determine the location of a transmitter by recording the time that a single transmitted waveform is received at several different locations. If the positions of these locations are known and their clocks are adequately synchronized, then by using the time of arrival (TOA), the position of the transmitter and the time of its transmission can be determined [1]. This can work without the cooperation of the transmitter.

Multilateration algorithms can be broadly grouped into three categories: iterative, closed-form non-linear, and linear. Iterative methods [2], [3], [4] often perform well but take longer to compute than closed-form methods and can converge to the wrong solution [5]. Closed-form non-linear methods, such as quadratic methods [6], [7], explicitly give the multiple solutions produced by iterative methods but are not always scalable and are not generally compatible with other forms of information such as AOA [8], [9], [10], [11], [12] and FDOA [13], [14], [15]. Linear methods are easily expanded to include additional data [14], [16], but require at least one extra measurement [17], [18] and can be less stable when the linear equations are ill-conditioned.[1] When there are enough measurements[2] the three families of methods have similar accuracy.

One shortcoming of most closed-form solutions to the multilateration problem is that they do not have a way of incorporating or exploiting any a priori information about the target's location to calculate its position [19]. From the perspective of a single sensor, the target can lie anywhere on a sphere.The motivation for this paper is to incorporate an a priori position estimate as a constraint on the multilateration problem. This is done by using linear approximations of the spherical surfaces, at the a priori estimate position. This geometry has been employed to determine the maximum accuracy of a localization algorithm [20], but not as a way of updating a location estimate.

For the purposes of this paper, the creation and maintenance of the a priori estimate is not considered a part of the algorithm. The initial a priori estimate can come from a wide range of sources. This can include location via surveillance radar, location via unconstrained multilateration, or using self-reported position information from transponder systems such as ADS-B. This method also be used to create improved positions of objects in a swarm, using an average or group position as the a priori estimate.

This paper presents the derivation of the algorithm. Section III analyzes the sources of error, including measurement error and error created because the true position differs from the estimate. This later error sets a minimum accuracy for the algorithm which can be iteratively improved. Section IV compares the new algorithm with linear TDOA multilateration across a range of wide area multilateration scenarios.

II. Differential Multilateration Algorithm

In this paper, vectors representing a point in space are written in bold, e.g., $\mathbf{a}$ and vectors representing a difference between two points are written with an overbar, e.g., $\bar{c}$.

Conventional multilateration uses a set of distances from a set of known points to a target to determine the position of the target. The target is located at the intersection of a set of spheres. If the target is far from the known points then the spheres can be approximated by planes tangent to the sphere at or near the location of the target. Choosing the point of tangency requires some *a priori* knowledge of the position of the target.

The proposed new algorithm takes an estimated target position $\mathbf{b}$ and uses it to produce planar approximations of

Manuscript received 10 April 2023; revised 26 June 2023; accepted 1 August 2023. Date of publication 15 August 2023; date of current version 12 September 2023. *(Corresponding author: Eric Widdison.)*

The authors are with the Department of Electrical and Computer Engineering, Brigham Young University, Provo, UT 84602 USA (e-mail: ewiddiso@byu.edu).

Digital Object Identifier 10.1109/TRS.2023.3305471

[1]The numerical stability problem can also affect iterative and quadratic methods. Many iterative and quadratic methods also involve matrix inversion and become unstable when those matrices are ill-conditioned.

[2]Three dimensional TDOA multilateration requires at least 5 measurements, corresponding to the 3 spatial dimensions, the unknown clock offset, and one extra degree of freedom to help linearize the equations.

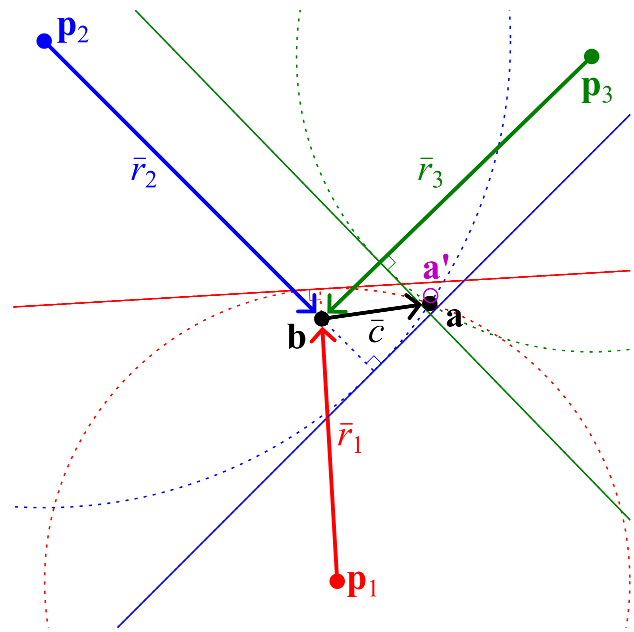

Fig. 1. The multilateration scenario. Points in space are shown as dots while vectors representing the difference between two points are shown as arrows. The solid lines are the planar approximations of the spheres passing through **a**, shown as dotted lines. This method places the target at the incircle of the triangle they form, marked as $\mathbf{a}'$.

the spheres used in conventional multilateration. The planar approximations of the spheres are perpendicular to the vectors from the known points $\mathbf{p}_i$ to the estimated position **b**, which is adjusted based on the measured pseudodistance and estimated transmitter pseudodistance, as shown in Fig. 1.

Let $\mathbf{a} = \mathbf{b} + \bar{c}$ be the unknown position of a transmitter relative to the known estimate **b** and let $\mathbf{p}_i, i = 1, \ldots, N$ be the positions of N receivers. The transmitter emits a signal at unknown time t_a which is received at $\mathbf{p}_i$ at time t_i. Pseudodistances

$$\begin{aligned} d_a &= t_a \nu \\ d_i &= t_i \nu \end{aligned} \tag{1}$$

are calculated, where ν is the propagation speed of the signal, which is typically the speed of light, c. The distance between transmitter and receiver is then $|\mathbf{a} - \mathbf{p}_i| = d_i - d_a$.

For each point $\mathbf{p}_i$, let $\bar{r}_i = \mathbf{b} - \mathbf{p}_i$ be the radial vector for that point. The planar approximation of a sphere of radius $(d_i - d_a) = d\left|\bar{r}_i\right|$ centered at $\mathbf{p}_i$, perpendicular to $\bar{r}_i$, is the set of points orthogonal to $\bar{r}_i$ at $\mathbf{p}_i + d\bar{r}_i$ such that

$$\left\langle (\mathbf{a} - \mathbf{p}_i) - d\bar{r}_i, \bar{r}_i \right\rangle = 0. \tag{2}$$

This is equivalent to

$$\left\langle \mathbf{a}, \bar{r}_i \right\rangle + d_a\left|\bar{r}_i\right| = d_i\left|\bar{r}_i\right| + \left\langle \mathbf{p}_i, \bar{r}_i \right\rangle, \tag{3}$$

which can be normalized by dividing by $|\bar{r}_i|$ to produce

$$\left\langle \mathbf{a}, \hat{r}_i \right\rangle + d_a = d_i + \left\langle \mathbf{p}_i, \hat{r}_i \right\rangle \tag{4}$$

where $\hat{r}_i = \bar{r}_i / |\bar{r}_i|$ is the unit vector in the direction of $\bar{r}_i$. In 3-dimensional space this is a linear equation of four unknowns. These equations, taken across four or more points, can be expressed as a matrix equation of the form

$$\begin{aligned} \mathbf{A} &= \left[\begin{array}{c|c} \hat{r}_1^{\mathrm{T}} & 1 \\ \vdots & \vdots \\ \hat{r}_N^{\mathrm{T}} & 1 \end{array}\right] \\ \mathbf{x} &= \begin{bmatrix} \mathbf{a}' \\ d_a' \end{bmatrix} \\ \mathbf{y} &= \begin{bmatrix} d_1 + \left\langle \mathbf{p}_1, \hat{r}_1 \right\rangle \\ \vdots \\ d_N + \left\langle \mathbf{p}_N, \hat{r}_N \right\rangle \end{bmatrix} \\ \mathbf{A}\mathbf{x} &= \mathbf{y} \end{aligned} \tag{5}$$

where $\mathbf{a}'$ is the calculated position and d_a' is the calculated pseudodistance associated with the signal transmission time. The unknowns can be calculated directly as $\mathbf{x} = \mathbf{A}^{-1}\mathbf{y}$ if **A** is square or via least squares as $\mathbf{x} = \left(\mathbf{A}^{\mathrm{T}}\mathbf{A}\right)^{-1}\mathbf{A}^{\mathrm{T}}\mathbf{y}$.

This method produces estimates of the target position that are at least as accurate as those from traditional multilateration as long as the measurement error is small enough relative to the error due to using a planar approximation of the multilateration spheres. The general stability of this method is analyzed in Sec. III and the errors due to approximating the spheres as planes is analyzed in Sec. III-B.

A. Two Dimensional Algorithm

This algorithm, as written, can be used in an D-dimensional space, but here is only used for $D = 2, 3$. For a target and reference points in 3 dimensions, at least four reference points are required to determine the location of the target. The $D = 2$ case requires only 3 reference points, along with some care to implement correctly.

In a 2-dimensional implementation the assumption is that the target lies on a 2-dimensional plane. Since 2-dimensional scenarios typically constrain the solution space and not the locations of receivers, the positions of the reference points may be somewhere other than directly on that plane. The algorithm uses the propagation speed in the plane, which in this case needs to account for the difference between the slant range between the transmitter and receiver, and the projection of that range onto the plane. If $\bar{r}_i = \begin{bmatrix} x_i & y_i & z_i \end{bmatrix}^{\mathrm{T}}$ and the target is assumed to lie in the xy plane then the projected pseudodistance

$$d_i = t_i \nu_i = t_i \nu \cos \phi_i \tag{6}$$

where

$$\tan \phi_i = \frac{z_i}{\sqrt{x_i^2 + y_i^2}}. \tag{7}$$

Alternately, this is

$$d_i = t_i \nu \left(\frac{\sqrt{x_i^2 + y_i^2}}{\left|\bar{r}_i\right|} \right). \tag{8}$$

With this adjustment of the pseudodistance, compared to Eq. 1, the 2 dimensional algorithm can be implemented using Eq. 5 with **A** of size $N \times 3$.

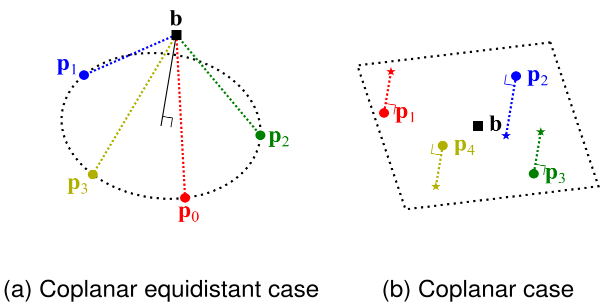

Fig. 2. A depiction of numerically unstable scenarios, with the estimate position marked as a square and the receiver positions marked as circles. In (a), the coplanar equidistant case, the receivers all lie on a circle and the estimate lies on the axis of symmetry of that circle. In (b) the receivers all lie on the same plane as the estimate. The points marked by stars are included to show that the receiver positions are equivalent to non-coplanar points that have been projected onto a single plane.

III. Numerical Stability

A. Unstable Cases

There are two cases where the $\mathbf{A}$ matrix is singular. When the receivers are all coplanar[3] and equidistant from the estimate point (the coplanar equidistant case, i.e. the receivers lie on a circle and the estimate point is on the line that is equidistant from all points on the circle, Fig. 2a), or when the receivers are coplanar with the estimate point (the coplanar case, Fig. 2b). In both of these cases, the $\mathbf{A}$ matrix is not full rank and cannot be inverted. It is possible for a scenario to experience both instability conditions at the same time.

Multilateration algorithms cannot generally work when the receivers are all coplanar. The proposed algorithm is numerically stable when the receivers are coplanar as long as the *a priori* estimate point is not also coplanar with them and the receivers are not all equidistant from the estimate point.

The coplanar equidistant case is equivalent to all the receivers lying on a circle with the estimate point on the line perpendicular to the circle and passing through the center. To see why this case does not produce a full rank matrix, consider the case where the radial unit vectors are all of the form $\hat{r}_i = \left[\, r\cos\theta_i \;\; r\sin\theta_i \;\; z \,\right]^{\mathrm{T}}$, where θ_i is the bearing from the estimate point to the ith receiver. This produces the matrix

$$\mathbf{A} = \begin{bmatrix} r\cos\theta_1 & r\sin\theta_1 & z & 1 \\ \vdots & \vdots & \vdots & \vdots \\ r\cos\theta_N & r\sin\theta_N & z & 1 \end{bmatrix}. \tag{9}$$

The right two columns of $\mathbf{A}$ have the same value in each row, so the columns are multiples of each other. This means the matrix $\mathbf{A}$ has, at most, rank 3, when it needs to be rank 4 to be inverted and produce a valid estimate of $\mathbf{a}'$.

If the receivers lie on any plane other than one parallel to the xy plane then the $\mathbf{A}$ matrix can be converted into this form by a coordinate transformation, which means that the matrix is rank deficient for any set of coplanar receivers that are equidistant from the transmitter.

[3]In this section, the term "coplanar" is based on a 3 dimensional algorithm. More generally, these instability cases require that $D+1$ receivers lie in a $D-1$ dimensional subspace of a D dimensional space. In the 2 dimensional case this condition only applies when at least three points are colinear and equidistant from the reference point. However, three points cannot be colinear and all equidistant from a fourth point. Therefore the coplanar equidistant condition cannot apply in 2 dimensions.

In the second unstable case, the receivers and estimate points are all coplanar. This can be examined by considering the case where the radial vectors all lie on the xy plane and are of the form $\hat{r}_i = \left[\, x_i \;\; y_i \;\; 0 \,\right]^{\mathrm{T}}$. This produces the $\mathbf{A}$ matrix

$$\mathbf{A} = \begin{bmatrix} x_1 & y_1 & 0 & 1 \\ \vdots & \vdots & \vdots & \vdots \\ x_N & y_N & 0 & 1 \end{bmatrix}. \tag{10}$$

With one column equal to zero, this matrix is also deficient. As with the coplanar equidistant receiver case, any set of receivers that are coplanar with the estimate can, with a coordinate transformation, be put in this form and is rank deficient.

These instability cases depend only on the receiver locations and the estimate point. One way to ensure that these conditions are never met is to ensure that the receivers are not coplanar. If the target's position can be assumed to be out of the plane containing the receivers, for example, if the target is an airplane with some minimum altitude, then it is sufficient to ensure that the receivers do not lie in a circle. With a large number of receivers this is unlikely to occur accidentally, but when only 4 receivers are used some care should be taken in choosing suitable locations for the receivers.

B. Planar Approximation Error

In this algorithm, the use of planes to approximate spheres introduces some error into the results. When radii of the spheres are large then this estimate is relatively accurate locally around $\mathbf{b}$. The approximation is less accurate when the target is farther from the radial line passing through the *a priori* estimate. This section quantifies that error.

Using this algorithm, the correct position is calculated when the measured pseudodistance[4] d_i is adjusted to match the projection of the target's true position onto the radial vector. The measured pseudodistance represents the slant range to the target, which is the hypotenuse of a right triangle with the projected distance as one of its legs. The difference between these two distances is the planar approximation error, or planar error e_i, as shown in Fig. 3.

The distance to the target is $d_i = |\mathbf{a} - \mathbf{p}_i| = \left|\bar{r}_i + \bar{c}\right|$ and the length of the projection of $\mathbf{a} - \mathbf{p}_i = \bar{r}_i + \bar{c}$ onto $\bar{r}_i$ is

$$\tilde{d}_i = \frac{\langle \bar{r}_i + \bar{c}, \bar{r}_i \rangle}{\left|\bar{r}_i\right|}. \tag{11}$$

The planar error is

$$\begin{aligned} e_i &= d_i - \tilde{d}_i = \left|\bar{r}_i + \bar{c}\right| - \frac{\langle \bar{r}_i + \bar{c}, \bar{r}_i \rangle}{\left|\bar{r}_i\right|} \\ e_i &= \sqrt{\langle \bar{r}_i + \bar{c}, \bar{r}_i + \bar{c} \rangle} - \frac{\langle \bar{r}_i + \bar{c}, \bar{r}_i \rangle}{\left|\bar{r}_i\right|} \\ e_i &= \sqrt{\left|\bar{r}_i\right|^2 + 2\langle \bar{r}_i, \bar{c} \rangle + \left|\bar{c}\right|^2} - \left|\bar{r}_i\right| - \frac{\langle \bar{r}_i, \bar{c} \rangle}{\left|\bar{r}_i\right|}. \end{aligned} \tag{12}$$

[4]To improve the readability of the derivations in this section, we ignore the transmitter pseudodistance, and assume that the pseudodistance d_i is a true distance, with $d_a = 0$. This does not affect the results of the derivation. If $d_a \neq 0$ then the first line in Eq. 12 starts $e_i = d_i - d_a - (\tilde{d}_i - d_a) = d_i - \tilde{d}_i \ldots$, with the rest of the derivation following identically.

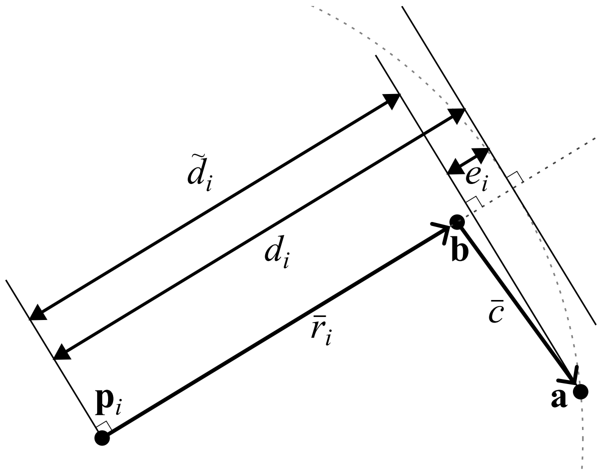

Fig. 3. The planar error and pseudodistance for a single receiver. The planar error e_i in this figure is exaggerated by the small value of $|\bar{r}_i|$ and relatively large displacement between the target $\mathbf{a}$ and the radial vector $\bar{r}_i$.

The radical term can be approximated by factoring out $\left|\bar{r}_i\right|^2$ and using the binomial expansion

$$(1+a)^n = 1 + na + \frac{1}{2!}n(n-1)a^2 + \frac{1}{3!}n(n-1)(n-2)a^3 + \cdots . \tag{13}$$

Because $\left|\bar{r}_i\right| \gg \left|\bar{c}\right|$, the first order terms and the first half of the second order terms are sufficient to estimate the error.[5]

$$e_i \approx \left|\bar{r}_i\right|\left(1 + \frac{\langle \bar{r}_i, \bar{c}\rangle}{\left|\bar{r}_i\right|^2} + \frac{\left|\bar{c}\right|^2}{2\left|\bar{r}_i\right|^2} - \frac{\langle \bar{r}_i, \bar{c}\rangle^2}{2\left|\bar{r}_i\right|^4}\right) - \left|\bar{r}_i\right| - \frac{\langle \bar{r}_i, \bar{c}\rangle}{\left|\bar{r}_i\right|}$$

$$e_i \approx \frac{\left|\bar{c}\right|^2 - \langle \hat{r}_i, \bar{c}\rangle^2}{2\left|\bar{r}_i\right|}. \tag{14}$$

This is equal to the square of the length of the component of $\bar{c}$ that is orthogonal to $\bar{r}_i$. Since $\left|\bar{c}\right| \geq \left|\langle \hat{r}_i, \bar{c}\rangle\right|$, the planar error is within the range

$$0 \leq e_i \leq \frac{\left|\bar{c}\right|^2}{2\left|\bar{r}_i\right|} \tag{15}$$

If $\bar{c}$ follows a D-dimensional multivariate normal distribution with variance σ_c^2, i.e., each element of $\bar{c}$ follows a normal distribution with zero mean and variance σ_c^2, then the expected value of e_i is

$$\begin{aligned} E(e_i) &= E\left(\frac{\left|\bar{c}\right|^2 - \langle \hat{r}_i, \bar{c}\rangle^2}{2\left|\bar{r}_i\right|}\right) \\ &= \frac{1}{2\left|\bar{r}_i\right|}\left[E\left(\left|\bar{c}\right|^2\right) - E\left(\langle \hat{r}_i, \bar{c}\rangle^2\right)\right] \\ &= \frac{1}{2\left|\bar{r}_i\right|}\left[D\sigma_c^2 - \sigma_c^2\right] \\ &= \frac{(D-1)\sigma_c^2}{2\left|\bar{r}_i\right|}. \end{aligned} \tag{16}$$

[5]The algorithm is not suitable when $\left|\bar{r}_i\right| \gg \left|\bar{c}\right|$ is not true. The worst case considered in this paper is shown in Fig. 6 where the average value of $|\bar{r}_i|/|\bar{c}|$ is $10/\sqrt{3}$. In that scenario, the algorithm in Eq. 5 is unable to reduce the standard deviation of the error in the calculated position below 100 m.

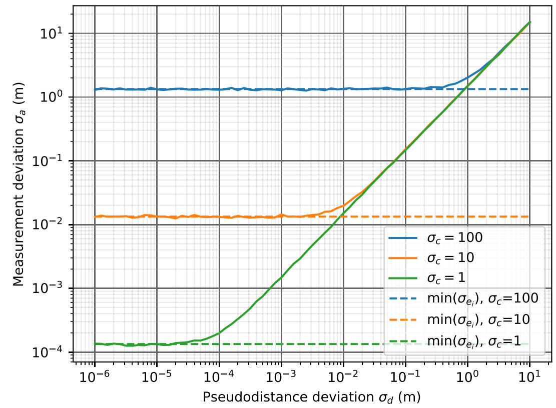

Fig. 4. Simulations of planar noise with 4 receivers and different levels of σ_c. The theoretical minimum measurement error is marked by the horizontal dotted lines. The receivers are located in a tetrahedron, centered on the transmitter, with each receiver 7.5 km from the transmitter.

This agrees with the mean of a chi-squared distribution with $D-1$ degrees of freedom [21, pp.62-63], scaled by σ_{e_i}, and agrees with the way that Eq.14 subtracts one degree of freedom from the D-dimensional normal distribution of $\bar{c}$. The variance of the planar error is given by scaling the chi-squared variance of $2(D-1)$ by $\sigma_{e_i}^2$ to get

$$\sigma_{e_i}^2 = \frac{(D-1)\sigma_c^4}{2\left|\bar{r}_i\right|^2}. \tag{17}$$

When $D=3$, this gives $\sigma_{e_i} = \sigma_c^2/\left|\bar{r}_i\right|$.

When solving the equations, the d_a' term should account for any bias due to the mean value of e_i. The degradation of the calculated position is due to the variance of the error terms, $\sigma_{e_i}^2$. This combines with the variance of the measurement error, $\sigma_{d_i}^2$, to produce the total error in the calculated position. This means that the position error is dominated by the planar error when $\sigma_{d_i}^2 < \sigma_{e_i}^2$, which creates a performance floor which can be seen in Figs. 4-9. The floor occurs at the level where the planar error limits the accuracy of the measured position, which corresponding to $\sigma_d \geq \sigma_{e_i}$, as seen in Fig. 4.

C. Statistical Optimization

To improve the performance of this algorithm, we consider the statistical effects of measurement noise and planar error on the computations.

Let the noisy measurements be $\tilde{d}_i = d_i + n_i + e_i$ where n_i is a Gaussian random variable representing the noise, and let $\mathbf{n} = [n_1, \ldots, n_N]^{\mathrm{T}}$ be a vector of the measurement noise. The noisy measurement also includes the planar error term, which can be concatenated to form the planar error vector $\mathbf{e} = [e_1, \ldots, e_N]^{\mathrm{T}}$. We can assume that the measurement noise is zero mean and uncorrelated with the planar error, with covariance

$$\mathrm{E}(\mathbf{n}\mathbf{n}^{\mathrm{T}}) = \mathbf{Q}_n. \tag{18}$$

The mean of $\mathbf{e}$ is

$$\boldsymbol{\mu}_{\mathbf{e}} = \mathrm{E}(\mathbf{e}) = \begin{bmatrix} \frac{(D-1)\sigma_c^2}{2|\bar{r}_1|} \\ \vdots \\ \frac{(D-1)\sigma_c^2}{2|\bar{r}_N|} \end{bmatrix} = \frac{D-1}{2}\sigma_c^2\mathbf{r}', \tag{19}$$

where $\mathbf{r}' = [|\bar{r}_1|^{-1}, \ldots, |\bar{r}_N|^{-1}]^{\mathrm{T}}$. Because the planar error has a non-zero mean we need the correlation matrix $\mathbf{R}_e = E[\mathbf{e}\mathbf{e}^{\mathrm{T}}]$ rather than the covariance matrix $\mathbf{Q}_e = E[(\mathbf{e}-\boldsymbol{\mu}_e)(\mathbf{e}-\boldsymbol{\mu}_e)^{\mathrm{T}}]$. The elements of $\mathbf{R}_e$ are[6]

$$\begin{aligned}R_{e,ij} &= E[e_i e_j] = \mathrm{E}\left[\frac{|\bar{c}|^2 - \langle \hat{r}_i, \bar{c}\rangle^2}{2|\bar{r}_i|}\frac{|\bar{c}|^2 - \langle \hat{r}_j, \bar{c}\rangle^2}{2|\bar{r}_j|}\right]\\ &= \frac{1}{4|\bar{r}_i||\bar{r}_j|}\mathrm{E}\Big[|\bar{c}|^4 - |\bar{c}|^2\Big(\langle \hat{r}_i, \bar{c}\rangle^2 + \langle \hat{r}_j, \bar{c}\rangle^2\Big)\\ &\quad + \langle \hat{r}_i, \bar{c}\rangle^2\langle \hat{r}_j, \bar{c}\rangle^2\Big]\\ &= \frac{\sigma_c^4}{4|\bar{r}_i||\bar{r}_j|}\Big(2D + D^2 - 2(D+2) + 2\langle \hat{r}_i, \hat{r}_j\rangle^2 + 1\Big)\\ &= \frac{D^2 - 3 + 2\langle \hat{r}_i, \hat{r}_j\rangle^2}{4|\bar{r}_i||\bar{r}_j|}\sigma_c^4. \end{aligned} \tag{20}$$

This noise model changes Eq. 5 to

$$\begin{aligned}\mathbf{A} &= \left[\begin{array}{c|c}\hat{r}_1^{\mathrm{T}} & 1\\ \vdots & \vdots\\ \hat{r}_N^{\mathrm{T}} & 1\end{array}\right]\\ \tilde{x} &= \begin{bmatrix}\tilde{a}'\\ \tilde{d}'_a\end{bmatrix}\\ \tilde{y} &= \begin{bmatrix} d_1 + \langle \mathbf{p}_1, \hat{r}_1\rangle\\ \vdots\\ d_N + \langle \mathbf{p}_N, \hat{r}_N\rangle\end{bmatrix} + \mathbf{n} + \mathbf{e}\\ \mathbf{A}\tilde{x} &= \tilde{y}\end{aligned} \tag{21}$$

where $\tilde{x}, \tilde{a}, \tilde{d}_a, \tilde{y}$ are the noisy versions of $\mathbf{x}, \mathbf{a}, d_a, \mathbf{y}$ respectively.

The position error is therefore equal to

$$\boldsymbol{\psi} = \tilde{x} - \mathbf{x} = \mathbf{x} + \mathbf{A}^{\dagger}(\mathbf{n}+\mathbf{e}) - \mathbf{x} = \mathbf{A}^{\dagger}(\mathbf{n}+\mathbf{e}) \tag{22}$$

where $\mathbf{A}^{\dagger}$ is the inverse or pseudoinverse of $\mathbf{A}$. The expected value of this error is

$$\begin{aligned}\mathrm{E}(\boldsymbol{\psi}) &= \mathbf{A}^{\dagger}[\mathrm{E}(\mathbf{n}) + \mathrm{E}(\mathbf{e})]\\ &= \mathbf{A}^{\dagger}\boldsymbol{\mu}_{\mathbf{e}}.\end{aligned} \tag{23}$$

The variance of the position error can be expressed as

$$\begin{aligned}\mathrm{E}(\boldsymbol{\psi}\boldsymbol{\psi}^{\mathrm{T}}) &= \mathrm{E}\Big[\mathbf{A}^{\dagger}(\mathbf{n}+\mathbf{e})(\mathbf{n}+\mathbf{e})^{\mathrm{T}}\mathbf{A}^{\dagger\mathrm{T}}\Big]\\ &= \mathbf{A}^{\dagger}\mathbf{Q}_n\mathbf{A}^{\dagger\mathrm{T}} + \mathbf{A}^{\dagger}\mathbf{Q}_e\mathbf{A}^{\dagger\mathrm{T}}.\end{aligned} \tag{24}$$

Using weighted least squares (WLS), this is

$$\mathrm{E}(\boldsymbol{\psi}\boldsymbol{\psi}^{\mathrm{T}}) = (\mathbf{A}^{\mathrm{T}}\mathbf{W}\mathbf{A})^{-1}\mathbf{A}^{\mathrm{T}}\mathbf{W}(\mathbf{Q}_n + \mathbf{Q}_e)\mathbf{W}\mathbf{A}(\mathbf{A}^{\mathrm{T}}\mathbf{W}\mathbf{A})^{-1}. \tag{25}$$

This suggests that the total error can be minimized by applying WLS with

$$\mathbf{W} = (\mathbf{Q}_n + \mathbf{R}_e)^{-1} \tag{26}$$

and

$$\mathbf{x} = \left(\mathbf{A}^{\mathrm{T}}\mathbf{W}\mathbf{A}\right)^{-1}\mathbf{A}^{\mathrm{T}}\mathbf{W}\mathbf{y}. \tag{27}$$

In practice, incorporating the $\mathbf{R}_e$ planar error correlation does not significantly improve the calculated position estimate, as shown in Fig. 5. In some cases, where σ_d^2 is small and $\sigma_c^2/|\bar{r}_i|$ is large, the $\mathbf{Q}_n + \mathbf{R}_e$ matrix is ill-conditioned. Therefore, we suggest using $\mathbf{W} = \mathbf{Q}_n^{-1}$ rather than the value from Eq. 26, and address the effects of planar error by the iterative approach presented in Sec. III-D.

The equations in this algorithm are nearly identical to those used by Lee [20] to determine the geometric dilution of precision (GDOP) of a multilateration scenario. The only difference is that Lee used the true position of the target while this uses an approximation. This means that when the estimate error σ_c^2 is small the measurement error asymptotically approaches the GDOP. For multilateration where the pseudodistance errors are zero mean Gaussian variables, the Cramér-Rao lower bound (CRLB) is equal to the GDOP [22].

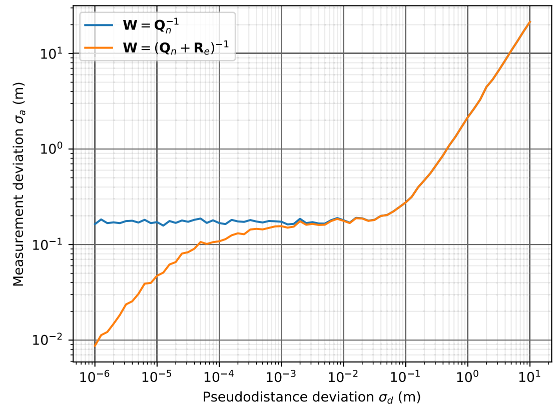

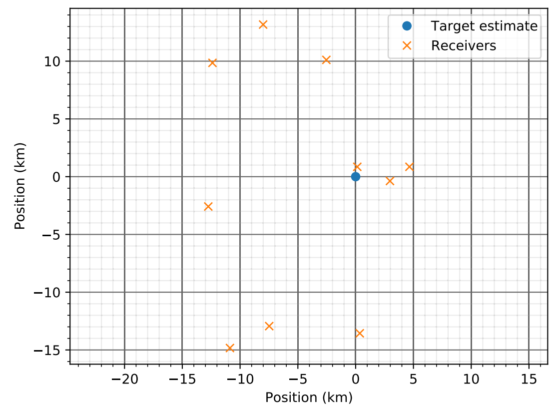

Fig. 5. Demonstration of weighted least squares solution accuracy, with 10 receivers randomly distributed as shown and $\sigma_c = 10$ m. Note that the weighted solutions are identical when the measurement error dominates ($\sigma_d > 0.01$ m), and that including $\mathbf{R}_e$ in the weighting only makes relatively small gains except in cases with extremely low measurement errors ($\sigma_d < 1$ mm).

D. Multi-Pass Algorithm

The planar bias error can be reduced by using the calculated position to adjust the pseudodistances and then recalculate. This can be done using the direct calculation in Eq. 12 or the approximation in Eq. 14, using $\mathbf{a}'$ to determine an estimate of $\bar{c}$, which in turn is used to estimate the errors. The updated pseudodistances are $d_i' = d_i - e_i$ and the updated position $\mathbf{a}''$ is given by

$$\mathbf{x}' = \begin{bmatrix}\mathbf{a}''\\ d_a''\end{bmatrix}$$

[6] $\mathrm{E}(|\bar{c}|^4) = (2D + D^2)\sigma_c^4 = D(D+2)\sigma_c^4$, $\mathrm{E}(|\bar{c}|^2\langle \hat{r}_i, \bar{c}\rangle^2) = (D+2)\sigma_c^4$, and $\mathrm{E}(\langle \hat{r}_i, \bar{c}\rangle^2\langle \hat{r}_j, \bar{c}\rangle^2) = (2\langle \hat{r}_i, \hat{r}_j\rangle^2 + 1)\sigma_c^4$. The first value is derived from the variance and mean of the chi square distribution. The others are determined experimentally.

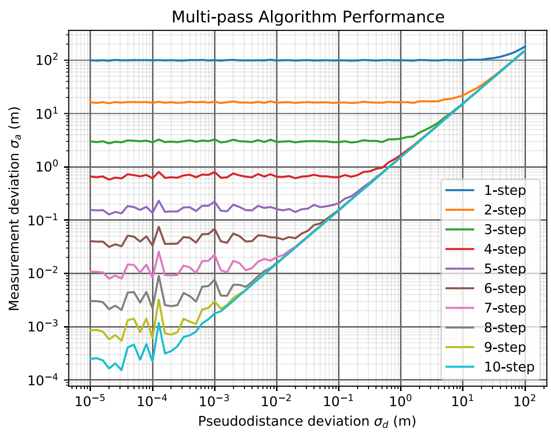

Fig. 6. Improvements in position from iterating the algorithm. The receivers are located in a regular tetrahedron centered on and 10 km away from the estimate point. The position accuracy is $\sigma_c = 1\,\text{km}$.

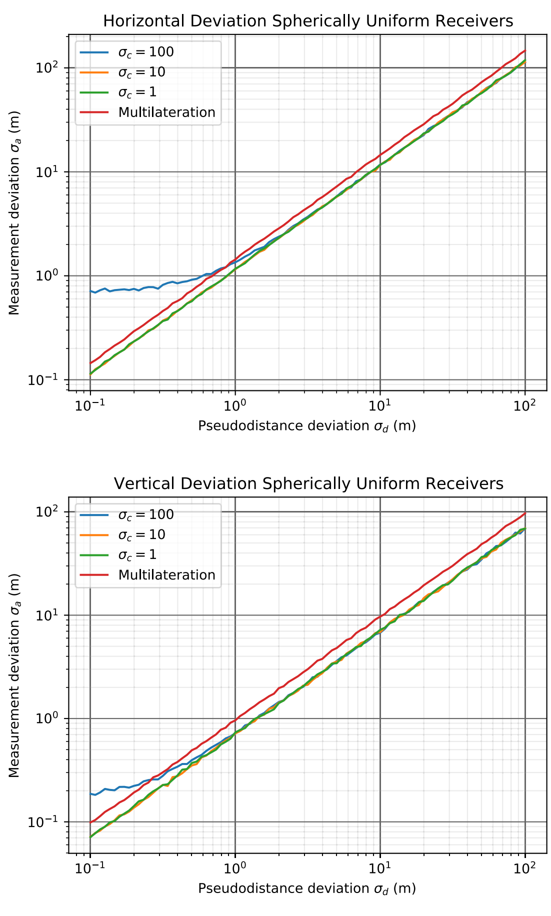

Fig. 7. Comparison of the differential multilateration algorithm with traditional multilateration with spherically uniform receivers. The new algorithm matches or exceeds performance except when planar error exceeds the measurement error.

$$\mathbf{y}' = \begin{bmatrix} d_1' + \langle \mathbf{p}_1, \hat{r}_1 \rangle \\ \vdots \\ d_N' + \langle \mathbf{p}_N, \hat{r}_N \rangle \end{bmatrix}$$

$$\mathbf{A}\mathbf{x}' = \mathbf{y}' \tag{28}$$

Because $\mathbf{A}$ is unchanged from the original algorithm, the second pass can reuse the same $\mathbf{A}^\dagger$ from the first pass, which reduces the computational cost of performing multiple passes.

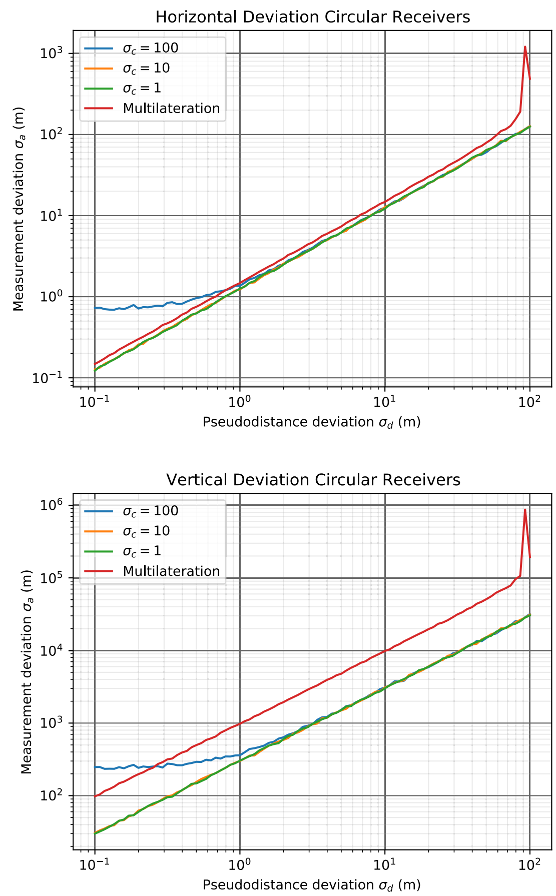

Fig. 8. Comparison of the differential multilateration algorithm with traditional multilateration with receivers in a nearly planar circular arrangement. This scenario is ill-conditioned for both methods, with only the small vertical deviations in receiver locations preventing both algorithms from producing singular matrices. The conventional multilateration algorithm became unstable with $\sigma_d > 100\,\text{m}$.

The second pass reduces the minimum measurement error by a factor of roughly $\sigma_c/|\bar{r}_i|$.

This step can be iterated more than once. Each time the original distances are updated using the new calculated position.

$$d_i^{(n+1)} = d_i - \left(\left| \mathbf{a}^{(n)} - \mathbf{p}_i \right| - \left\langle \mathbf{a}^{(n)} - \mathbf{p}_i, \hat{r}_i \right\rangle \right). \tag{29}$$

As the algorithm is iterated, the average error is reduced. Fig. 6 shows the algorithm's performance against a target with $\sigma_c = 1\,\text{km}$ and four receivers in a tetrahedral formation at a distance of 10 km from the reference point. The results are shown for 1 through 10 passes of the algorithm. After eight iterations (the first pass and seven update passes) the average planar error is less than the level for $\sigma_c = 10\,\text{m}$ with one pass under the same conditions. If the multi-pass algorithm is used then it should be stopped when $|\mathbf{a}^{(n+1)} - \mathbf{a}^{(n)}| < \epsilon$ for some value of ϵ, or after some number of iterations, whichever comes first. The multi-pass algorithm should only be used when the variance of the measurement error is very small.

IV. Performance Verification

To evaluate the performance of this algorithm we compare it to the linear multilateration approach from [17], using the optimal weighting as given in equations (11) through (14a). This is compared to the single-pass method as given in Eq. 27.

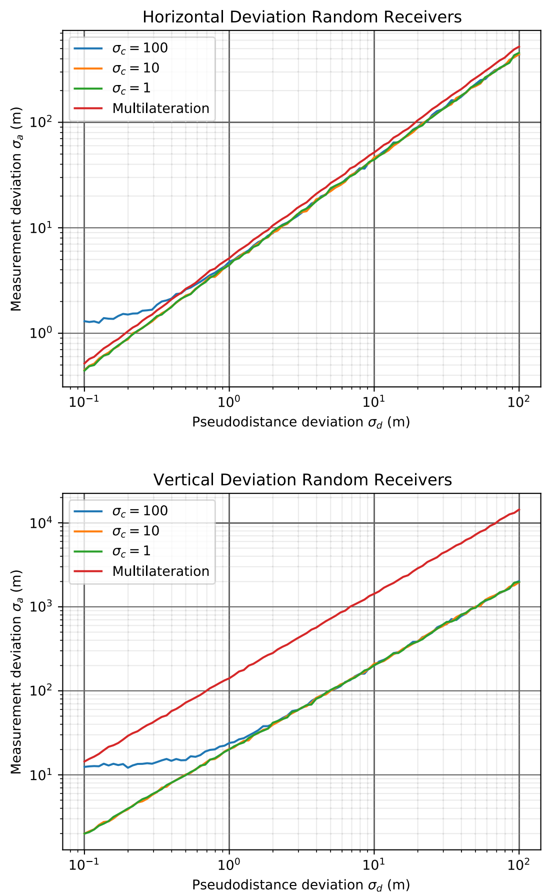

Fig. 9. Comparison of the differential multilateration algorithm with traditional multilateration with receivers randomly located in a 30 km × 30 km × 500 m box, centered 1 km below the estimated target position **a**. The new algorithm performed significantly better whenever the planar error was not the dominant source of measurement variance.

We apply these methods to three different scenarios, each using five receivers, showing horizontal and vertical errors on separate graphs. The scenarios are:

- spherically uniform, with receivers spread equally around a sphere [23] centered on the transmitter, shown in Fig. 7,
- circular, with receivers spread evenly in a circle around the transmitter, which is above the center of the circle, with some random vertical perturbation to prevent both algorithms from having singular matrices, shown in Fig. 8, and
- random, with receivers randomly distributed in a box of size 30 km × 30 km × 500 m, shown in Fig. 9.

The specific receiver locations are given in Table I. The transmitter is located at $\mathbf{a} = [0, 0, 0]^T$ in the spherically uniform scenario and at $\mathbf{a} = [0, 0, 1000]^T$ meters in the other two scenarios.

In every scenario, when the measurement noise variance was greater than the variance of the planar error the proposed algorithm performed better than traditional linear multilateration. The performance difference was especially pronounced in the circular scenario where the receivers are nearly coplanar and traditional linear multilateration has very poor accuracy vertically [24], [25].

TABLE I

RECEIVER LOCATIONS FOR PERFORMANCE VERIFICATION SCENARIOS. ALL FIGURES ARE GIVEN IN METERS

	Spherical		
point	x	y	z
$\mathbf{p}_1$	0	0	8000
$\mathbf{p}_2$	12000	0	0
$\mathbf{p}_3$	-5500	9526	0
$\mathbf{p}_4$	-4500	-7794	0
$\mathbf{p}_5$	0	0	-10000
	Circular		
point	x	y	z
$\mathbf{p}_1$	9500	0	-3
$\mathbf{p}_2$	3090	9511	-9
$\mathbf{p}_3$	-8090	5878	12
$\mathbf{p}_4$	-8090	-5878	6
$\mathbf{p}_5$	3090	-9511	9
	Random		
point	x	y	z
$\mathbf{p}_1$	12653	-1716	108
$\mathbf{p}_2$	7384	14813	67
$\mathbf{p}_3$	7896	6170	-99
$\mathbf{p}_4$	9637	-7515	182
$\mathbf{p}_5$	6563	2165	-36

V. CONCLUSION

This algorithm improves on traditional mutlilateration algorithms at obtaining an accurate 3-dimensional position in typical wide area multilateration scenarios. This comes at the cost of requiring an initial measurement and a target tracking algorithm to maintain the quality of the estimate. It is more numerically stable in typical wide area multilateration scenarios than traditional multilateration. This method reduces the number of measurements required by one, allowing for 3-dimensional localization with only four measurements instead of at least five for linear TDOA multilateration.

The key benefit of this algorithm is that it is well-suited for incorporation into a tracking algorithm. At any point in time the calculation of the estimate is linear, allowing for tracking with a simple Kalman filter rather than one of the non-linear extensions. It can also be employed for tracking swarms of objects where a central point within the swarm can act as an estimate for the position of an individual transmitter, and each calculated transmitter location contributes to the estimate of the swarm position.

This algorithm is based on having an *a priori* estimate for the location of a target. As such it requires that an initial position be available. This can be acquired with a different multilateration algorithm or by using some other sensor such as a radar. The accuracy of the algorithm is limited when the estimate is not accurate enough. The statistics, in Eq. 17, and simulations, in Fig. 6, show that in a wide area multilateration scenario the variance of the estimate error can be quite large without irreparably degrading the performance of the algorithm.

This algorithm is naturally suited for a tracking algorithm. It uses an estimate of the current position of an object to calculate an updated position, and all the calculations are linear functions. A Kalman filter should be able to both track the target and provide quality estimates of updated positions for use with future samples.

This algorithm could be used to measure and possibly track individual objects in a swarm. A traditional radar may not be able to distinguish individual objects in a swarm, but by using the radar's position as the estimate for the swarm as a whole, and then applying this algorithm to signals sent between members of the swarm, it may be possible to determine the positions of individual objects.

References

[1] J. J. Caffery and G. L. Stuber, "Overview of radiolocation in CDMA cellular systems," *IEEE Commun. Mag.*, vol. 36, no. 4, pp. 38–45, Apr. 1998, doi: 10.1109/35.667411.

[2] W. Foy, "Position-location solutions by Taylor-series estimation," *IEEE Trans. Aerosp. Electron. Syst.*, vols. AES-12, no. 2, pp. 187–194, Mar. 1976, doi: 10.1109/TAES.1976.308294.

[3] I. A. Mantilla-Gaviria, M. Leonardi, J. V. Balbastre-Tejedor, and E. D. L. Reyes, "On the application of singular value decomposition and Tikhonov regularization to ill-posed problems in hyperbolic passive location," *Math. Comput. Model.*, vol. 57, nos. 7–8, pp. 1999–2008, Apr. 2013, doi: 10.1016/j.mcm.2012.03.004.

[4] J. Kennedy and R. Eberhart, "Particle swarm optimization," in *Proc. IEEE Int. Conf. Neural Netw.*, vol. 4. Nov. 1995, pp. 1942–1948, doi: 10.1109/ICNN.1995.488968.

[5] J. Fresno, G. Robles, J. Martínez-Tarifa, and B. Stewart, "Survey on the performance of source localization algorithms," *Sensors*, vol. 17, no. 11, p. 2666, Nov. 2017, doi: 10.3390/s17112666.

[6] S. Bancroft, "An algebraic solution of the GPS equations," *IEEE Trans. Aerosp. Electron. Syst.*, vols. AES-21, no. 1, pp. 56–59, Jan. 1985, doi: 10.1109/TAES.1985.310538.

[7] R. Bucher and D. Misra, "A synthesizable VHDL model of the exact solution for three-dimensional hyperbolic positioning system," *VLSI Design*, vol. 15, no. 2, pp. 507–520, Jan. 2002.

[8] L. Cong and W. Zhuang, "Hybrid TDOA/AOA mobile user location for wideband CDMA cellular systems," *IEEE Trans. Wireless Commun.*, vol. 1, no. 3, pp. 439–447, Jul. 2002, doi: 10.1109/TWC.2002.800542.

[9] Y. Zhao, Z. Li, B. Hao, J. Si, and P. Wan, "Bias reduced method for TDOA and AOA localization in the presence of sensor errors," in *Proc. IEEE Int. Conf. Commun. (ICC)*, May 2017, pp. 1–6, doi: 10.1109/ICC.2017.7997043.

[10] Z. Liu, Y. Zhao, K. Jin, D. Hu, R. Wang, and Y. Zhao, "Algebraic distributed source localisation algorithm using TDOA and AOA measurements," *J. Eng.*, vol. 2019, no. 19, pp. 5962–5966, Oct. 2019.

[11] E. Widdison and D. G. Long, "Hybrid multilateration and triangulation," *Positioning*, vol. 12, no. 1, pp. 1–15, 2021, doi: 10.4236/pos.2021.121001.

[12] Y. Zhou, Y. Wang, R. Nie, Q. Cheng, and G. Zhu, "Optimal location method of spontaneous data fusion based on TDOA/AOA," in *Proc. China Ocean Acoust. (COA)*, Harbin, China, 2021, pp. 885–889, doi: 10.1109/COA50123.2021.9519960.

[13] K. C. Ho and Y. T. Chan, "Geolocation of a known altitude object from TDOA and FDOA measurements," *IEEE Trans. Aerosp. Electron. Syst.*, vol. 33, no. 3, pp. 770–783, Jul. 1997, doi: 10.1109/7.599239.

[14] K. C. Ho and W. Xu, "An accurate algebraic solution for moving source location using TDOA and FDOA measurements," *IEEE Trans. Signal Process.*, vol. 52, no. 9, pp. 2453–2463, Sep. 2004, doi: 10.1109/TSP.2004.831921.

[15] R. Ramlall, J. Chen, and A. L. Swindlehurst, "Non-line-of-sight mobile station positioning algorithm using TOA, AOA, and Doppler-shift," in *Proc. Ubiquitous Positioning Indoor Navigat. Location Based Service (UPINLBS)*, Corpus Christi, TX, USA, 2014, pp. 180–184, doi: 10.1109/UPINLBS.2014.7033726.

[16] K. C. Ho and M. Sun, "Passive source localization using time differences of arrival and gain ratios of arrival," *IEEE Trans. Signal Process.*, vol. 56, no. 2, pp. 464–477, Feb. 2008, doi: 10.1109/TSP.2007.906728.

[17] Y. T. Chan and K. C. Ho, "A simple and efficient estimator for hyperbolic location," *IEEE Trans. Signal Process.*, vol. 42, no. 8, pp. 1905–1915, Aug. 1994, doi: 10.1109/78.301830.

[18] A. Norrdine, "An algebraic solution to the multilateration problem," *presented at the Int. Conf. Indoor Positioning Indoor Navigat.*, Sydney, NSW, Australia, Nov. 2012.

[19] M. Pourkhaatoun and S. A. Zekavat, "TOA estimation techniques: A comparison," in *Handbook Position Location*, S. A. Zekavat and R. M. Buehrer, Eds. Hoboken, NJ, USA: Wiley, 2019, pp. 237–267, doi: 10.1002/9781119434610.ch7.

[20] H. Lee, "Accuracy of range-range and range-sum multilateration systems," *IEEE Trans. Aerosp. Electron. Syst.*, vols. AES-11, no. 6, pp. 1346–1361, Nov. 1975, doi: 10.1109/TAES.1975.308191.

[21] L. L. Scharf *Statistical Signal Processing: Detection, Estimation, and Time Series Analysis*. Reading, MA, USA: Addison-Wesley, 1991.

[22] J. Chaffee and J. Abel, "GDOP and the Cramer–Rao bound," in *Proc. IEEE Position, Location Navigat. Symp. (PLANS)*, Las Vegas, NV, USA, Apr. 1994, pp. 663–668, doi: 10.1109/PLANS.1994.303374.

[23] O. R. Musin and A. S. Tarasov, "The Tammes problem for $N = 14$," *Experim. Math.*, vol. 24, no. 4, pp. 460–468, Oct. 2015, doi: 10.1080/10586458.2015.1022842.

[24] D. Fontanelli, F. Shamsfakhr, and L. Palopoli, "Cramer–Rao lower bound attainment in range-only positioning using geometry: The G-WLS," *IEEE Trans. Instrum. Meas.*, vol. 70, pp. 1–14, 2021, doi: 10.1109/TIM.2021.3122521.

[25] R. M. Buehrer and S. Venkatesh, "Fundamentals of time-of-arrival-based position location," in *Handbook Position Location*, S. A. Zekavat and R. M. Buehrer, Eds. Hoboken, NJ, USA: Wiley, 2019, pp. 199–236, doi: 10.1002/9781119434610.ch6.

Eric Widdison (Member, IEEE) received the B.S. degree in electrical engineering and mathematics and M.Eng. degree in electrical engineering from Utah State University, Logan, UT, USA, in 2003, and the Aerospace and Defense M.B.A. degrees from the University of Tennessee, Knoxville, TN, USA, in 2013. He is currently pursuing the Ph.D. degree with Brigham Young University, Provo, UT, USA.

He has been a Civilian Engineer with the United States Air Force since 2004. He has been an Adjunct Instructor at the Electrical and Computer Engineering Department, Weber State University, Ogden, UT, USA, since 2014.

David G. Long (Life Fellow, IEEE) received the Ph.D. degree in electrical engineering from the University of Southern California in 1989. From 1983 to 1990, he worked for NASA's Jet Propulsion Laboratory (JPL) where he developed advanced radar remote sensing systems. While at JPL he was the Project Engineer on the NASA Scatterometer (NSCAT) project which flew from 1996 to 1997. He also managed the SCANSCAT project, the precursor to SeaWinds which was flown in 1999 on QuikSCAT, in 2002 on ADEOS-II, and in 2014 on the International Space Station. He is currently a Professor in the Electrical and Computer Engineering Department, Brigham Young University, where he teaches upper division and graduate courses in communications, microwave remote sensing, radar, and signal processing and is the Director of the BYU Center for Remote Sensing. He is the principal investigator on several NASA-sponsored research projects in remote sensing. He has over 400 publications in various areas including signal processing, radar scatterometry, and synthetic aperture radar. His research interests include microwave remote sensing, radar theory, space-based sensing, estimation theory, signal processing, and mesoscale atmospheric dynamics. He has received the NASA Certificate of Recognition several times and is an Associate Editor for IEEE GEOSCIENCE AND REMOTE SENSING LETTERS.